Chapter 2
Experimental and Theoretical Methods

2.1 Chemicals and Instruments

The chemicals used for catalyst preparation are shown in Table 2.1.

The gases used in the experiments are shown in Table 2.2.

The instruments used in the experiments are shown in Table 2.3.

2.2 Measurements of Model Surfaces

2.2.1 Ultra-High Vacuum (UHV) System

The UHV system is shown in Fig. 2.1, which is composed of two layers of stainless chamber.

Inside the chamber, the single crystal was placed at the center by directly spot-welding the crystal to two tantalum posts, for resistive heating and cooling with liquid nitrogen. A chromel-alumel K-type thermocouple was welded to the back of the crystal for temperature measurements. The UHV system is equipped with metal source, sputter gun, Auger electron spectroscopy (AES), low-energy electron diffraction (LEED), and mass spectrometer (MS) [1].

2.2.2 Preparation of Single-Crystal Surfaces

The Pd(111) (Princeton Scientific, 99.99%, 2 mm thick and 10 mm in diameter) surface was cleaned using sputtering-annealing cycles. The Ni-terminated, NiPdPd (111) and Pd-terminated, PdNiPd(111) bimetallic surfaces were prepared by controlling the current of the Ni source, the temperature of the Pd(111) surface and the

© Springer Science+Business Media Singapore 2017

R. Hou, *Catalytic and Process Study of the Selective Hydrogenation of Acetylene and 1,3-Butadiene*, Springer Theses, DOI 10.1007/978-981-10-0773-6_2

Table 2.1 Chemicals used for catalyst preparation

Chemical	Standard	Purchase source
$Pd(NO_3)_2{\cdot}2H_2O$	99.9%	Alfa Aesar
$Ni(NO_3)_2{\cdot}6H_2O$	98%	Alfa Aesar
$PdCl_2$	99.9%	Alfa Aesar
HCl	AR	Beijing Chemical Works
γ-Al_2O_3	–	Alfa Aesar
SiO_2	–	Alfa Aesar
SiO_2	AR	Beijing Yili Fine Chemicals
CeO_2	99%	Alfa Aesar
ZrO_2	99%	Alfa Aesar
TiO_2	99.5%	Xiya Reagent
$(NH_4)_2MoO_4$	99.997%	Alfa Aesar
$C_6H_{12}N_2PO_3$	–	Linzhou Keneng Material Technology
(NMP)	CP	Sinoreagent
$C_{10}H_{22}$	CP	Sinoreagent

Table 2.2 Gases used in the experiments

Gas	Formula	Standard	Purchase source
Acetylene	C_2H_2	High purity	Dongfang Gases
Hydrogen	H_2	≥99.999%	Beiwen Gases
Nitrogen	N_2	≥99.999%	Beiwen Gases
Air	O_2/N_2	High purity	Beiwen Gases
5% 1,3-butadiene in nitrogen	5% C_4H_6/N_2	High purity	Beiwen Gases
4% hydrogen in nitrogen	4% H_2/N_2	High purity	Beiwen Gases
Methane	CH_4	High purity	Beiwen Gases
1% oxygen in nitrogen	1% O_2/N_2	High purity	Beiwen Gases

Table 2.3 Instruments used in the experiments

Instrument	Version/model	Purchase source
Electronic analytical balance	JA503B	Shanghai Yueping
Ultrasonic cleaner	KQ100DB	Kunshan Ultrasonic
Heating and drying oven	DHG-9035A	Shanghai Yiheng Technology
Muffle furnace	SX-G07103	Tianjin Zhonghuan Oven
Gas chromatography	GC7900	Shanghai Tianmei Tech.
GC-column	HP-Al/S PLOT	Angilent
Autoclave	GS-0.25/17.5	Weihai Chemical Machinery
Heating magnetic stirrer	DF-101S	Zhengzhou Changcheng
Precision pressure gauge	KY2010	Beijing Kaihangweiye Tech.
Point welding machine	250 dp/230	Miyachi Unitek
Thermocouple wire	spal-005-100	Omega
Tungsten mesh	40,924	Alfa Aesar

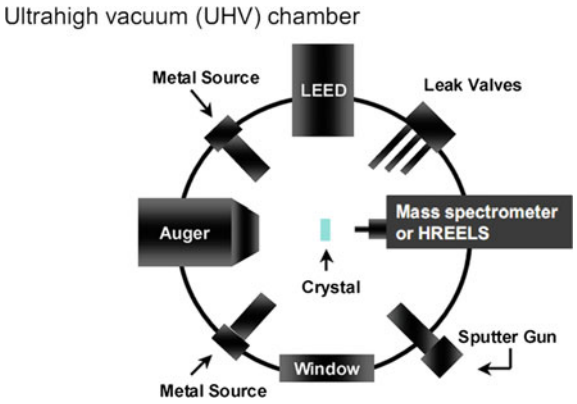


Fig. 2.1 UHV system

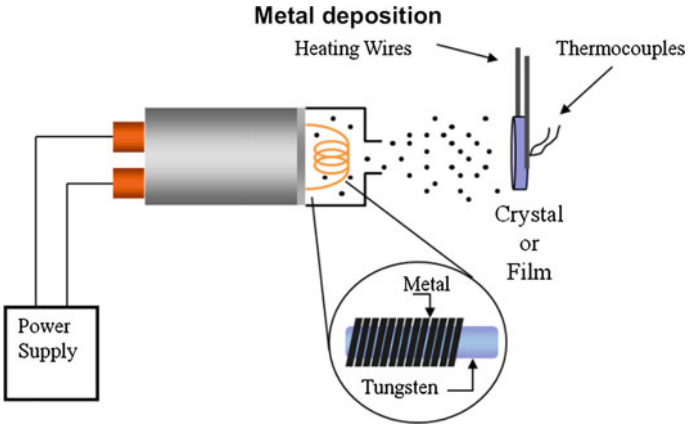


Fig. 2.2 Preparation of single-crystal surfaces

deposition time. The deposition process is shown in Fig. 2.2. The NiPdPd(111) surface was prepared by depositing Ni onto the Pd(111) surface while the surface was maintained at 300 K. The PdNiPd(111) surface was obtained by annealing the NiPdPd(111) surface at 600 K.

2.2.3 Temperature-Programmed Desorption (TPD)

In the TPD experiment, the single-crystal surface was firstly cooled to 120 K by liquid nitrogen; the gases were introduced into the UHV chamber and were allowed to adsorb on the crystal surface at the very low temperature; the single-crystal

surface was then heated at 3 K/s and the mass spectrometer (MS) was used to detect the desorbed gas-phase concentration. The mass balance was calculated by accounting the TPD desorption peaks, and the residues on the crystal surface was analyzed by AES.

2.3 Density Functional Theory (DFT) Calculations

All DFT calculations of binding energies were performed with the Vienna ab initio Simulation Package (VASP) [2–5]. The PW 91 functional [6] was used in the generalized gradient approximation (GGA) [7] calculation and a kinetic cutoff energy of 396 eV was chosen for the plane wave truncation. The surfaces were modeled using a periodic 4 × 4 unit cell, and the calculations used a 3 × 3 × 1 Monkhorst-Pack k-point grid. The clean Pd(111) surface was modeled by adding six equivalent layers of vacuum onto four Pd layers, in which the two bottom layers were frozen at metal distances of 2.80 Å in each layer and 2.3 Å between the layers, while the top two layers were allowed to relax to reach the lowest energy configuration. The Pd-terminated bimetallic surface, designated as PdNiPd(111), was derived by replacing the second layer of Pd atoms with Ni atoms. The binding energy of adsorbed molecules on the surface was calculated by subtracting the energies of the bare slab and of the free molecule from the total energy of the slab plus the adsorbed molecule. The configurations from VASP calculations were further optimized using the Cambridge Serial Total Energy Package (CASTEP) suite of programs to identify the transition state and calculate the activation energy for each reaction step.

2.4 Catalyst Preparation

2.4.1 Supported Catalyst

The supported catalysts were prepared by the incipient wetness impregnation method. An aqueous precursor solution was prepared by dissolving the desired amounts of metal salts in an amount of water just sufficient to fill the pores of 3 g of the support. The precursor solution was then added to the support by dropwise addition and was stirred thoroughly between droplets.

The Pd–Ni catalysts used in Chaps. 3 and 4 were dried at 100 °C for 10 h and calcined at 290 °C for 2 h. A ramp rate of 0.4 °C/min was used up to 100 and 0.8 °C/min up to 290 °C. A co-impregnation synthesis procedure was used for the bimetallic catalysts to produce the greatest extent of bimetallic bond formation, as verified previously for supported Pt–Ni catalysts [8]. The corresponding monometallic Ni and Pd catalysts were prepared to serve as control samples. The

Table 2.4 Temperature program and gas environment in the carburization

Step	Starting Temp./°C	Ending Temp./°C	Gas environment	Time/min
1	RT	600	20% CH_4/H_2	285
2	600	600	20% CH_4/H_2	120
3	600	600	H_2	60
4	600	30	H_2	Natural cooling
5	30	RT	1% O_2/N_2	360

compositions of the synthesized catalysts are as follows: 1.51 wt% Ni/γ-Al_2O_3, 0.91 wt% Pd/γ-Al_2O_3, and 1.51 wt% Ni-0.91 wt% Pd/γ-Al_2O_3, corresponding to a Ni:Pd atomic ratio of 3:1. The catalysts were reduced at 450 °C before use.

The 0.01% Pd/LSA-SiO_2 catalyst used in Chap. 6 was dried at 100 °C for 1 h and calcined at 400 °C for 4 h at the ramp rate of 5 °C/min. The precursor solution of H_2PdCl_4 was prepared by dissolving the desired amounts of equimolar $PdCl_2$ (99.9%, Alfa Aesar) and HCl (AR, Sinopharm) in deionized water. The reduction temperature was 200 °C.

The SCILL (supported catalyst with ionic liquid layer) was prepared by impregnating the ionic liquid onto the reduced catalyst and was dried at 80 °C overnight.

2.4.2 Mo_2C-Based Catalyst

The Mo_2C-based catalysts were prepared by the carburization of MoO_3 in CH_4/H_2. The MoO_3 was obtained by the calcination of ammonium molybdate at 350 °C for 6 h. When preparing Ni/Mo_2C, proper amount of $Ni(NO_3)_2$ was firstly impregnated with MoO_3, and the impregnated catalyst was dried and calcined as stated in Sect. 2.4.1 for Pd–Ni catalysts.

The carburization was carried out in a tubular furnace (internal diameter 60 mm). The calcined MoO_3 or Ni/MoO_3 was placed into a porcelain boat and the boat was placed in the center of the furnace. The temperature program and the gas environment for each step of the carburization are shown in Table 2.4

2.5 Catalyst Characterization

2.5.1 SEM

SEM (JSM 7401, JEOL) was used to measure the catalyst. The scan mode was LEI at an electron emission voltage of 3 kV and a current of 20 μA.

2.5.2 TEM

TEM measurements were performed using a JEOL2010F equipped with a Schottky field emission gun at 200 keV. All TEM images were taken in scanning (STEM) mode with a 12-nm camera length and a 1-nm-diameter nanoprobe. The TEM samples were prepared by first reducing the catalyst samples, then grinding the reduced sample into fine powders and suspending them in acetone. Droplets of the suspension were placed onto a carbon-coated copper grid. The grid was dried overnight before loading the sample into the TEM.

2.5.3 XRD

The crystalline phase of the catalysts was characterized from 20° to 80° 2θ by a Bruker Advance D8 X-ray diffractometer with Cu K_α ($\lambda = 1.5418$ Å) monochromatic radiation. The samples were dried and ground before being loaded onto the XRD instrument.

2.5.4 TG-DTA

The hydrocarbon species deposited on the catalysts were analyzed by TG-DTA (NETZSCH STA 409PC). In the measurement, 20 mg catalyst was used and was heated up from 30 to 800 °C at a ramp rate of 20 °C/min in an oxygen flow of 50 mL/min.

2.5.5 Physisorption

The surface area of the support was determined by Brunauer–Emmett–Teller (BET) method using N_2 adsorption-desorption on an Autosorb-1-C instrument (Autosorb iQ and AsiQwin, Quantachrome).

2.5.6 CO-Chemisorption

The number of active sites on each catalyst was measured through CO uptake with an AMI-200ip (Altamira). A quartz reactor was loaded with 100 mg of catalyst and reduced in 40 sccm of 50% H_2 in He at 450 °C for 1 h. After reduction, the catalyst was cooled to room temperature in He before pulsing CO. The amount of CO

flowing out of the reactor was measured with a thermal conductivity detector. Each adsorbed CO molecule was assumed to correspond to one active site, which provided a means to quantitatively compare the number of active sites between catalysts.

2.5.7 XAFS

EXAFS measurements were used to confirm the presence of Pd–Ni bimetallic bonds. Measurements of the Pd K-edge were performed on the X18B beamline at the National Synchrotron Light Source (NSLS), Brookhaven National Laboratory. The catalyst samples were pressed into a pellet with a thickness twice the absorption length to maximize the signal-to-noise ratio. The catalysts were placed in a chamber as shown in Fig. 2.3. The catalysts were reduced in situ in 40 sccm of 50% H_2 in He at 450 °C for 1.5 h, and the EXAFS spectra were collected at room temperature. The EXAFS spectra were calibrated to the Pd K-edge energy from a Pd reference foil.

The X-ray signal was analyzed using the IFEFFIT 1.2.11 data analysis package (Athena, Aretmis, Atoms, and FEFF6) [9, 10]. The structural information was obtained by Fourier-transforming the absorbance signal into R-space and then fitting each data set to the theoretical standards generated in FEFF6 [11]. The theoretical monometallic photoelectron amplitude and phase were calculated for the bulk Pd fcc structure. The passive electron reduction factor S_0^2 was found to be 0.878 from fitting the Pd-foil data. The seven parameters used in the fitting procedure were the correction to the edge energy, the coordination numbers of the Pd–Pd and Pd–Ni bonds, corrections to their model interatomic distances, and the mean square deviations in interatomic distances (EXAFS Debye-Waller factors).

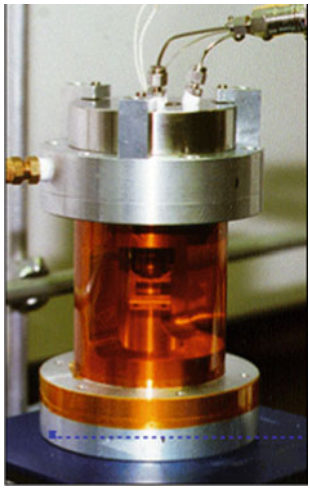


Fig. 2.3 Catalyst chamber for XAFS

2.6 Catalyst Evaluation

Three kinds of reactors were used in this thesis: the batch reactor equipped with a Fourier transform infrared (FT-IR) spectroscopy, the fixed-bed reactor equipped with gas chromatography (GC), and the slurry reactor with GC. The batch reactor was used to evaluate the catalyst activity and to obtain the kinetics; the fixed-bed reactor was used for steady-state operation, and for the evaluation of catalyst stability; the slurry reactor was used in the novel liquid-phase hydrogenation.

2.6.1 Batch Reactor

The batch reactor is composed of the in situ reaction chamber, the operation arm, and the gas pipelines, as shown in Fig. 2.4. FT-IR spectroscopy was used to monitor the gas-phase concentrations of reactants and products during the hydrogenation 1,3-butadiene. The reaction chamber is located in the IR detector cell and is connected with the operation arm, pumps, and the pipelines. The pipelines are in connection with gas cylinders and liquid sources. The FT-IR spectra were recorded with 4 cm^{-1} resolution using a Thermo Nicolet Nexus 470 spectrometer equipped with a mercury cadmium telluride (MCT-A) detector. Before each experiment, the catalyst was pressed onto a tungsten mesh and was connected to the heating and thermocouple systems.

For all FT-IR experiments, ~13.6 mg of supported catalyst was loaded into the IR cell, which was then evacuated for 12 h, until the system reached a pressure

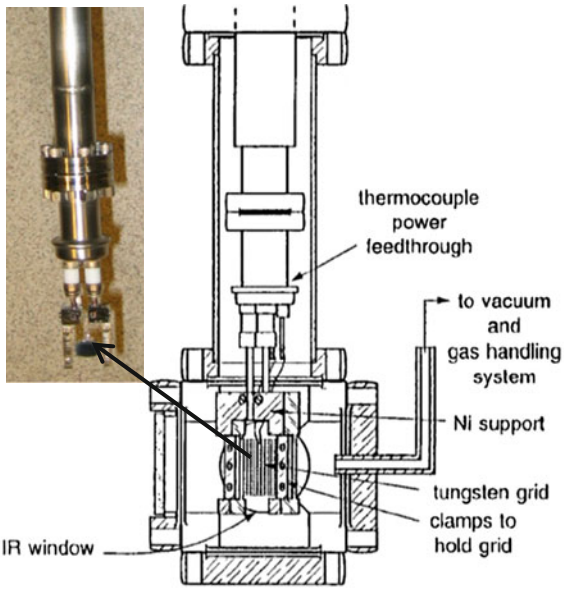


Fig. 2.4 Catalyst chamber for XAFS

below 10^{-6} Torr. The catalysts were reduced at 723 K in 30 Torr hydrogen for 30 min and the cell was then evacuated and a high-temperature flash (723 K) was performed to remove any surface species generated during the reduction period. The reduction cycle was repeated three times before performing the reaction experiments. After reducing the catalyst, a gas mixture was introduced into the reaction vessel simultaneously.

During the reaction, the gas-phase reactants and products were monitored by recording IR spectra (32 scans) every 30 s. The concentrations of the reactant and products were estimated using the absorbance intensities of their characteristic vibration modes as follows [8, 12, 13]: ν(C=C–C=C) at 1586 cm^{-1} for 1,3-butadiene,ν(C=C) at 1655 cm^{-1} for 1-butene, and$\nu(-CH_3)$ at 1466 cm^{-1} for *n*-butane. Because both 1-butene and butane contribute to the peak at 1466 cm^{-1}, in order to calculate the butane concentration, the intensity contributed by 1-butene should be substracted from the intensity at 1466 cm^{-1}:

$$\text{Intensity}_{\text{Butane (1466)}} = \text{Intensity}_{\text{Total (1466)}} - \alpha \cdot \text{Conc}_{\text{1-Butene (1655)}} \tag{2.1}$$

No 2-butene characteristic vibration modes (1697 and 1540 cm^{-1}) were found in the gas-phase products, as shown in Fig. 2.5. At present, we do not understand why 2-butene was not detected in the batch reactor. One potential explanation is that, in the batch environment, gas-phase products constantly undergo readsorption and reaction. More detailed study is needed to understand such phenomena; however, because our batch reactor results are primarily used for activity comparison, the absence of 2-butene does not affect the batch reactor conclusions of trends in hydrogenation activity (Fig. 2.5).

The concentrations of 1,3-butadiene, 1-butene, and butane were summed up for the estimation of carbon balance, as shown in Fig. 2.6. All carbon atoms were accounted for by performing a carbon balance, confirming the absence of 2-butenes and any other hydrocarbon fragments.

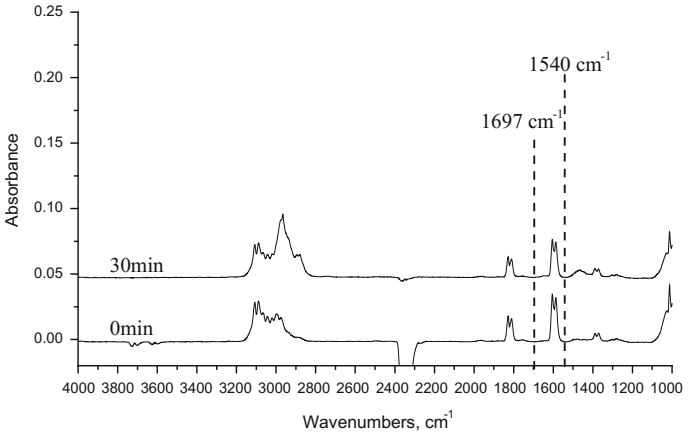


Fig. 2.5 IR spectra of the gas phase before and during the hydrogenation of 1,3-butadiene

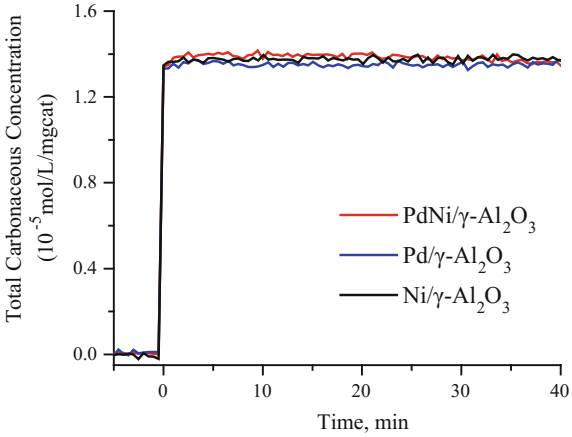


Fig. 2.6 Mass balance in the hydrogenation of 1,3-butadiene

2.6.2 Fixed-Bed Reactor

The fixed-bed reactor is shown in Fig. 2.7, composed of the inlet, reaction, control, and analysis sections. The reactant gases flow through filters, then to mass flow meters and finally to the fixed-bed reactor. The reactions studied in the thesis were performed at ambient pressure. The gas products were analyzed by a gas chromatograph by an auto six-way valve.

The fixed-bed reactor is 5 mm i.d. and 600 mm long. The catalyst was mixed with quartz particles in a ratio of 1:29 (100 mg catalyst and 2.9 g quartz particles). The temperature was monitored by a K-type thermocouple placed in the catalyst bed. Prior to reaction, the catalysts were reduced in hydrogen and then cooled to reaction temperature.

The outlet stream was analyzed online by a gas chromatograph equipped with a FID detector (GC 7900, Techcomp Ltd.) and an HP-Al/S PLOT column (Agilent, 30 m × 0.53 μm). The gas-phase carbon balance is above 95%. The selectivity of each product was calculated by dividing its concentration by the total products.

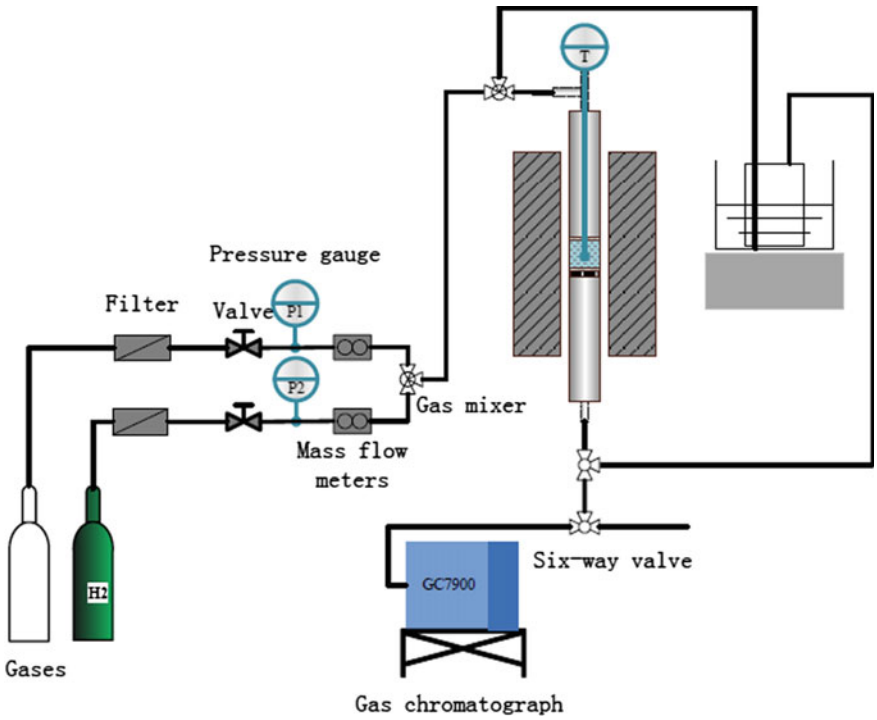


Fig. 2.7 Fixed-bed reactor system

2.6.3 Slurry Reactor

The liquid-phase hydrogenation of acetylene was carried out in a slurry reactor performed in a flat bottom flask with a magnetic stirrer and an oil bath to control the reaction temperature. The other parts were the same as in the gas-phase apparatus. The reduced catalyst and 80 mL NMP were placed in the flask. Experiments on the effect of stirring speed showed that under a low space velocity of 3600 ml/(gcat h), the acetylene conversion increased with increasing stirring speed until 600 rmp. In all the following experiments, a stirring speed of 700 rmp was used to eliminate the effect of gas–liquid mass transfer limitation.

2.7 Measurement of Solubility

The solubilities of acetylene and ethylene were measured isothermally from pressure decay observations using an apparatus similar to that used by Palgunadi et al. [14]. The apparatus is shown in Fig. 2.8. Two stainless steel vessels were used as

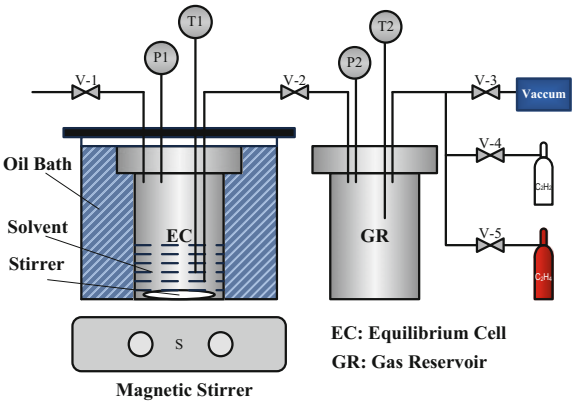


Fig. 2.8 Apparatus for the measurement of solubility

the equilibrium cell (EC) and gas reservoir (GR). The EC was placed in an oil bath with a magnetic stirrer and the GR was at room temperature. Both vessels were equipped with a thermocouple and a pressure gauge (0.4% in precision). The volumes of the two vessels with their tubes and fittings, V_{EC+TF1} and V_{GR+TF2}, were determined by the displacement of water with nitrogen gas (V_{EC+TF1} = 283 mL, V_{GR+TF2} = 291 mL).

The solubility was calculated with the following equation:

$$n_{sol} = n_{in} - n_{gas} = \frac{(P_2 - P_1)V_{GR}}{RT_2} - \left(\frac{(P_3 - P_1)(V_{EC} - V)}{RT_1} + \frac{(P_3 - P_1)V_{GR}}{RT_2}\right) \tag{2.2}$$

where the amount of gas was determined by the ideal gas law. An oil bath was used to control the temperature from 20 to 100 °C.

References

1. Yu WT, Barteau MA, Chen JG (2011) Glycolaldehyde as a probe molecule for biomass derivatives: reaction of C–OH and C=O functional groups on monolayer Ni surfaces. J Am Chem Soc 133(50):20528–20535
2. Ammann CM, Meehl GA, Washington WM et al (2003) A monthly and latitudinally varying volcanic forcing dataset in simulations of 20th century climate. Geophys Res Lett 30 (12):1657
3. Kresse G, Furthmuller J (1996) Efficient iterative schemes for ab initio total-energy calculations using a plane-wave basis set. Phys Rev B 54(16):11169–11186
4. Kresse G, Furthmuller J (1996) Efficiency of ab-initio total energy calculations for metals and semiconductors using a plane-wave basis set. Comput Mater Sci 6(1):15–50
5. Kresse G, Hafner J (1993) Abinitio molecular-dynamics for liquid-metals. Phys Rev B 47 (1):558–561

6. Perdew JP, Chevary JA, Vosko SH et al (1992) Atoms, molecules, solids, and surfaces—applications of the generalized gradient approximation for exchange and correlation. Phys Rev B 46(11):6671–6687
7. Teter MP, Payne MC, Allan DC (1989) Solution of Schrodinger-equation for large systems. Phys Rev B 40(18):12255–12263
8. Lonergan WW, Vlachos DG, Chen JG (2010) Correlating extent of Pt–Ni bond formation with low-temperature hydrogenation of benzene and 1,3-butadiene over supported Pt/Ni bimetallic catalysts. J Catal 271(2):239–250
9. Newville M (2001) IFEFFIT: interactive XAFS analysis and FEFF fitting. J Synchrot Radiat 8:322–324
10. Ravel B, Newville M (2005) ATHENA, ARTEMIS, HEPHAESTUS: data analysis for X-ray absorption spectroscopy using IFEFFIT. J Synchrot Radiat 12:537–541
11. Rehr JJ, Albers RC (2000) Theoretical approaches to x-ray absorption fine structure. Rev Mod Phys 72(3):621–654
12. Qi S, Yu W, Lonergan WW et al (2010) Low-temperature hydrogenation and dehydrogenation of 1, 3-cyclohexadiene on Pt/Ni bimetallic catalysts. Chin J Catal 31(8):955–960
13. Qi S, Yu W, Lonergan WW et al (2010) General trends in the partial and complete hydrogenation of 1,4-cyclohexadiene over Pt–Co, Pt–Ni and Pt–Cu bimetallic catalysts. ChemCatChem 2(6):625–628
14. Palgunadi J, Kim HS, Lee JM et al (2010) Ionic liquids for acetylene and ethylene separation: Material selection and solubility investigation. Chem Eng Process 49(2):192–198

http://www.springer.com/978-981-10-0772-9

Catalytic and Process Study of the Selective Hydrogenation of Acetylene and 1,3-Butadiene

Hou, R.

2017, XII, 141 p. 83 illus., 42 illus. in color., Hardcover
ISBN: 978-981-10-0772-9